Magnetic Resonance Elastography using an air ball-actuator

Tomokazu Numano[1,2], Yoshihiko kawabata[3], Kazuyuki Mizuhara[4], Toshikatsu Washio[2], Naotaka Nitta[2], Kazuhiro Homma[2]

[1]Department of Radiological Science, Graduate School of Human Health Science, Tokyo Metropolitan University
7-2-10, Higashiogu, Arakawa-ku, Tokyo, Japan
TEL +81-3-3819-1211
FAX +81-3-3819-1406
e-mail: t-numano@hs.tmu.ac.jp

[2]Human Technology Research Institute, National Institute of Advanced Industrial Science and Technology (AIST)

[3]Takashima Seisakusho Co.,Ltd

[4]Department of Mechanical Engineering, TOKYO DENKI UNIVERSITY

Abstract

The purpose of this study was to develop a new technique for a powerful compact MR Elastography (MRE) actuator based on a pneumatic ball-vibrator. This is a compact actuator that generates powerful centrifugal force vibrations via high speed revolutions of an internal ball using compressed air. This equipment is easy to handle due to its simple principles and structure. Vibration frequency and centrifugal force are freely adjustable via air pressure changes (air flow volume), and replacement of the internal ball. In order to achieve MRI compatibility, all parts were constructed from non-ferromagnetic materials. Vibration amplitudes (displacements) were measured optically by a laser displacement sensor. From a bench test of displacement, even though the vibration frequency increased, the amount of displacement did not decrease. An essential step in MRE is the generation of mechanical waves within tissue via an actuator, and MRE sequences are synchronized to several phase offsets of vibration. In this system, the phase offset was detected by a four-channel optical-fiber sensor, and it was used as an MRI trigger signal. In an agarose gel phantom experiment, this actuator was used to make an MR elastogram. This study shows that the use of a ball actuator for MRE is feasible.

Key Words: Magnetic resonance elastography; pneumatic ball-vibrator; actuator; mechanical waves; propagating waves

1. Introduction

Magnetic Resonance Elastography (MRE) [1-4] utilizes the fact that the shear wave propagation in biological tissue is related to material stiffness. Stiffness parameters such as the shear modulus may serve to distinguish between normal and abnormal tissues [5,6]. In recent years, MRE has been used for biomechanical assessment of tissue-engineered cartilage [7]. In conventional MRE, repetition time (TR) cycle shear motions are applied to the tissue of interest using external vibration sources of motion, and the resultant oscillating displacements are imaged into the MR phase images using negative-positive switching gradient lobes (motion-encoding gradient: MEG) inserted into conventional MR pulse sequences [1-4]. The MEG is placed after RF excitation of the sample and before measurement of the induced signal. The displacement of vibration is recorded on the MR phase image as the MR phase offset by manipulating the axes on which the MEGs are placed. For example, only the displacement of vibration occurring in the read-out direction will be sensitized to, and encoded into, the MR phase image. When the period of external vibration and the period of MEG are in agreement, the effect due to MEG serves as the maximum. In short, the implementation of MEG increases the sensitivity of the MRE pulse sequence to the displacement of wave penetration. The recorded wave images (MR phase images) were converted into shear stiffness images by using an inversion algorithm. The local frequency estimate (LFE) algorithm was used

routinely as an inversion algorithm [8].

The mechanical TR cyclic waves employed in MRE are typically in the low acoustic frequency range of 40 – 150Hz, and are often generated by a vibration device that is placed on the surface of the human body over the region of interest [9-12]. The high frequency (500Hz or more) vibration device is used to measure small biological samples [7,13]. These devices must be designed so as not to create artefacts or electromagnetic noise, and must be suitable for the high magnetic field of an MRI scanner. Investigators have described successful MRE vibration devices that are based on electromechanical, piezoelectric, and remote-pneumatic actuators. An electromechanical actuator works via the Lorentz force and utilizes the static magnetic field of the MRI magnet. Applying alternating currents to an annular coil generates motion. A maximal torque acts on the coil if the normal vector of its plane is perpendicular to the static magnetic field. The resultant periodic tilt is transformed for mechanical actuation using a pivoted rod. In this commonly used design, the orientation of the actuator coil restricts the directions available for mechanical excitation. A piezoelectric actuator-generated vibration is based on the piezoelectric properties of certain materials. Although high frequency vibration is possible by using a piezoelectric actuator, it only causes a small amount of displacement. A remote-pneumatic actuator is a widely used method of creating the required vibrations for MRE, utilizes the motion of the voice coils used in acoustic speaker systems. These speakers, with their own permanent magnets, have to be placed away from the MRI magnet, so this system requires an additional component to couple the vibration produced by the speakers to the tissue. One approach is to enclose the area around the speaker cone or its equivalent in order to use a long connecting tube to pneumatically conduct the harmonic pressure variations of the air into the scanner and to terminate the tube in a big stethoscope-like driver kept in contact with the tissue [11,14,15]. Remote-pneumatic actuators are easier to construct, cost less, and can be customized easily to account for in vivo applications such as liver [11,16,17], muscle [15,18,19], or breast MRE [9,10]. For low acoustic frequency ranges (120Hz or less), remote-pneumatic actuators can achieve an adequate number of wave penetration displacements. However, when the acoustic frequency increases (150Hz or more), the pneumatic actuator was difficult to achieve an adequate number of wave penetration displacement [14]. Furthermore, the penetration of high frequency waves is easily attenuated in the material. At the higher frequencies, the MR phase offset of the MRE sequence is decreased and it has a reduced shear wave sensitivity.

The decrease in the MR phase offset of the MRE sequence can be enhanced by increasing repetition of MEG or increasing the MEG gradient power. However, the repetition of MEG has an upper limit because the increased repetition of MEG extends the echo time (TE). Extensions of TE tend to decrease the signal to noise ratio (SNR), and increase the influence of magnetic susceptibility. In particular, the repetition of MEG cannot be increased when imaging short T2 relaxation components in a sample. The switching of the gradients induces an electrical current in conducting

tissues according to Faraday's law. In the MRE sequence for human studies, a rapidly changing magnetic field associated with the switching of magnetic field gradients can generate currents in tissue, which may exceed the nerve depolarization threshold and cause peripheral nerve stimulation (PNS). Therefore, the repetition of MEG and the MEG gradient power have an upper limit.

In this study, an air ball-actuator is introduced that allows the operator to maintain a range of displacement independent of frequency. To demonstrate the feasibility of the new actuator, MRE experiments on agarose gel phantoms are presented and the performance properties measured optically by a laser displacement sensor.

2. Materials and methods

2.1 Ball-actuator mechanism

Fig. 1 shows a picture of a prototype MRI-compatible ball-actuator. The concept for air ball-actuator was inspired by a pneumatic ball-vibrator. Pneumatic ball-vibrators are commonly used in industrial applications. Compressed air flows in through the tube connector (I). As a result, a vibration is generated due to the centrifugal force accompanied by rotation of the internal ball (II) in the circumferential direction of the raceway ring (III). Centrifugal force vibration and vibration frequency are changed by replacement of the internal ball (II), and operational air pressure. The air pressure (air flow volume) is controlled by the regulator. Physical property data for internal balls are summarized in Table 1. The actuator body is made from acrylic, and the built-in raceway ring (III) is made from polytetrafluoroethylene (PTFE). The four-channel optical-fiber sensor (IV) enabled the synchronization of four time vibration phase offsets. The optical-fiber sensor is one pair of a "sender" and a "receiver". Basically, a laser light is always transmitted to the light sensor "sender" from the optical signal operating system via an optical fiber, and irradiated downward in the actuator body. On the other hand, the light sensor "receiver", disposed opposite to the light sensor "sender", receives the light irradiated from the light sensor "sender" and feeds back the optical signal relating to the received light to the optical signal operating system. The light sensors' "sender" and "receiver" function only to irradiate the light and receive the irradiated light. Therefore, a light-emitting element as a light generating means for generating light by the application of voltage, and a light-receiving element as a light receiving means for converting the received light into the corresponding electrical signal, are installed in the operating system. Under these circumstances, when the motion in the circumferential direction of the internal ball (II) is conducted along the inner surface of the raceway ring (III), the light reception at the light sensor "receiver" is disturbed when the internal ball (II) is passed through the space between the light sensors' "sender" and "receiver" so that the electrical signal to be transmitted to the optical signal operating system relating to the received light at the light sensor "receiver" is stopped. On the other hand, since the motion in the circumferential direction of the internal ball (II) is continuously conducted in terms of time when the

MRE was produced, the electrical signal to be received at the operating system is stopped at a prescribed time. Therefore, the rotational velocity in the motion of the circumferential direction of the internal ball (II) can be monitored by measuring the time for each non-reception of the electrical signal and calculating the period of time, that is, the frequency for the non-reception of the electrical signal. The above-mentioned method operates via each channel, so the synchronization of four vibration phase offsets is possible. If the revolution speed of internal ball is extremely-stable, it should be possible to offset the synchronization from a single optical-fiber sensor to achieve any desired phase offset (by using delay time). But actually, since revolution speed of internal-ball is slightly fluctuated, the four vibration phase offset by using 4ch optical-fiber sensors (hardware-offset) is desirable. The compressed air introduced into the ball actuator is discharged outside from the silencer (V). The silencer mitigates exhaust noise, but exhaust efficiency and revolution speed falls. If humidity of the air was high, the mist separator could not remove as much of the moisture as possible from air. As a result, the filter of silencer was clogged with moisture. Then, the exhaust efficiency was getting worse and worse. Thus, we removed the silencer to make the high exhaust efficiency. This MRI-compatible ball-actuator has low friction of moving parts. In addition, heat generated due to moving parts is always reduced by an inflow of compressed air.

The centrifugal force of the ball-actuator can be calculated with the following equation:

$$F = M \times r \times \left(\frac{2\pi \times N}{60} \right)^2 \qquad (1)$$

where F is centrifugal (vibration) force ($kg \cdot m/s^2$), M is ball mass (kg), r is the rolling radius of the internal ball (m), and N is revolutions per minute (rpm). In theory, if the revolution speed of the internal ball (vibration frequency) rises, centrifugal (vibration) force will rise. This is the outstanding feature of the ball-actuator, and it maintains adequate amount of displacement, even if changing frequency vibrations. Centrifugal (vibration) force changes also with the weight and the diameters of internal ball. The relationship between the centrifugal force and internal ball type was calculated from the formula (1) and the result of calculation shows in Fig. 2. Each ball revolution is 6,000 rpm (vibration frequency is 100Hz). If the diameter of the internal ball is small (rolling radius is increased) and the ball is heavy, the centrifugal force will increase.

In theoretical formula, Eq.(1), the rotative speed (rpm) of internal ball can be easily controlled by the air flow volume. But practically, as the air flow volumes increase, more compressed air is entering the raceway ring chamber, and then the pressure of chamber is increase. As a result, in order to achieve and maintain the high rpm (high vibration frequency), higher pressure compressed air is necessary.

2.2 Ball-actuator system

Fig. 3. illustrates the experimental setup. Compressed air generated at the compressor (0.75LE-10.2S [0.75kW, 72l/min], HITACH, Tokyo, Japan) (I) was controlled as flow volume by the high-precision regulator (IR2020-02BG, SMC, Tokyo, Japan) (III), and introduced into the ball-actuator. The mist separator (AWM20-02GB, SMC, Tokyo, Japan) (II) removes moisture from compressed air. The air flow volume was measured by a thermal mass flowmeter (TF-901S, TOKYO KEISO, Tokyo, Japan) (IV). The rotational velocity of the internal ball (Fig. 1a II) was always monitored by a selected optical-fiber (Fig. 1a IV) and an optical signal operating system (V). All of the neighboring optical-fiber sensor positions are at right angles to each other. Exact vibration phase offset ($\pi/2$ vibration phase offset) becomes possible with this structure. Commonly-used a MRE actuator is triggered by the MRI sequence to synchronize the acquisition of the produced mechanical vibration. In the proposed ball-actuator application this occurs in an exact opposite way: the ball-actuator system is generating the synchronization pulse for the MRI scanner (Fig. 4b). To measure the characteristics of the ball-actuator, its triaxial accelerations were measured by a tri-axis XYZ accelerometer (KXM52-1050, Kionix, NY, USA; Fig. 5a), its vibration displacement was measured by a laser displacement sensor (LK-G35, KEYENCE, Tokyo, Japan; Fig. 5b), the air flow volume was measured by a thermal mass flowmeter, while a self-made simultaneous measurement system (LabVIEW, National Instruments, TX, USA) was used to record the displacement (or acceleration) and air flow volume. The ball-actuator performance assessment experiments were carried out outside the MRI magnet.

2.3 MRE experiments

All Magnetic Resonance imaging (MRI) data and MRE data were acquired on a 2.0-T animal experiment MR scanner system (Biospec 20/30, BRUKER, Karlsruhe, Germany) with a B-GA20 Gradient System that had a maximum gradient strength of ±100mT/m. The MR data acquisition, image reconstruction and pulse sequence development were performed with the ParaVision 4.0 (BRUKER) software system. A 140-mm-ID birdcage coil tuned to 85 MHz for proton resonance was used for all measurements. All elastograms were processed by Local Frequency Estimate (LFE) algorithm freeware (MRE/Wave, MAYO CLINIC). Fig. 4a shows a self-modified spin echo (SE) MRE sequence. This sequence combines motion-encoding gradients (MEG) with a spin echo imaging module. In this sequence, the MEG was applied symmetrically around a refocusing (180 degree RF) pulse and the period of external vibration and the period of MEG were in agreement. The SE-MRE sequence imaging parameters were a coronal or sagittal imaging plane, 12-cm field of view (FOV), 256×128 acquisition matrix (256×256 image matrix), 400-ms TR (technically, because MRI synchronizes with trigger from ball-actuator, TR becomes slightly longer than 400 ms; Fig. 4b), 26.4 or 29.3-ms TE, 5-mm slice thickness, 200 or 160Hz continuous vibration (12,000 or 9,600rpm of ball-actuator), one pair of 5.00 or 6.25-ms motion-encoding gradients (MEG), MEG capable of

being applied in any direction, and a 3-min 28-sec total acquisition time (four vibration phase offsets). All experiments were performed on an agarose gel phantom. Two types of phantom were prepared: one of the gel phantoms was made from 1.0% agarose (weight %) poured into a semi-rigid plastic container and the other spherical inclusion of 30 mm diameter was made from 1.25% agarose enclosed in the center. For both phantoms, using 3.0% agarose formed a hard crust on the surface for protection.

3. Results

3.1 Ball-actuator performance assessment experiments

The frequency characteristics of ball-actuator with different internal balls were examined in a bench test using a self-made simultaneous measurement system. Fig. 5 shows disposition of the experiment devices. Arrowed lines of Fig. 5a indicate the tri-axis XYZ accelerometer coordinate system, and it was loaded condition (impact absorption rubber mat). The displacements measured with the ball-actuator were in a loaded condition (approximately agarose-gel 2.8kg; Fig.5b). Fig. 6a. shows the change in vibration frequency (revolutions per minute: rpm / sixty-seconds) vs. flow volume rate for the different internal balls. The air ball-actuator requires the inertial ramp time (the frequency of vibration to become stable after the change of air flow volume). It takes five seconds before the vibration frequency and displacement becoming steady state. Following the increase in air flow volume, the vibration frequency was increased for every internal ball. Furthermore, the vibration frequency was influenced by the relationship between the ball diameter and ball weight. A lower density internal ball material produced a higher revolution speed and a vibration frequency increase. Fig. 6b. shows tri-axis acceleration vs. change in vibration frequency (rpm / sixty-seconds). Because the internal ball (5/16 PEEK) was rotate in accelerometer's Y-Z plane, the Y-axis acceleration denotes the same tendency of Z-axis. Since the Y-axis was slightly loaded condition compared with Z-axis, the acceleration of Y-axis was slightly less than Z-axis. In theory, the ball-actuator has not displacement (acceleration) for the X-axis direction. However, because the accessory of actuator (fiber cables, air flow-in tube, and cables of accelerometer, for example) was vibrated, it induces the vibration of the X-axis direction. Fig. 6c. shows the change in measured displacement vs. vibration frequency (rpm / sixty-seconds) for different internal balls. The increased displacement of the waves at 35 and 70 Hz are presumably the result of intrinsic resonances of the device itself. When the diameter of the internal ball was shorter (rolling radius is increased) and the ball was heavy, the displacement increased. Even though the vibration frequency increased, the amount of displacement was maintained at a certain value, except for sympathetic vibration.

3.2 MRE experiments

Since the air ball-actuator requires the inertial ramp time, in order to avoid the contamination of

unsteady state vibration, the ball-actuator makes continuous vibration throughout the entire MRE acquisition (one vibration phase offset). Furthermore, MRE acquisitions were started after ball-actuator generated steady state vibration. In all MRE experiments, we chose 5/16 PEEK because it was efficient for high rotative speed. Fig. 7 shows the uniform agarose gel phantom experimental results obtained for coronal slice orientations. The comparison of wave images (0, $\pi/2$, π, $3\pi/2$) reveals that the four time vibration phase offsets. The arrowed line indicates the direction of MEG. All of the neighboring optical-fiber sensor positions are at right angles to each other. Because of this sensor positions, when the vibration offset 0 (or $\pi/2$) of a wave image is compared with the vibration offset π (or $3\pi/2$), the pattern of share wave propagation in the agarose gel phantom is inverted. This result shows that the MRI-compatible ball-actuator gives closely synchronized signals. Fig. 8. compares the wave image of the imaging plane and the direction of MEG. These were wave images of the uniform agarose gel phantom with 160Hz vibration frequency. The arrowed line indicates the direction of MEG. In Fig. 8a, the shear waves propagate with an equally-spaced stripe pattern from the top to the bottom of the phantom. By reorienting MEG (Fig. 8b), the wave pattern was changed as a speckled pattern. By MEG direction normal to the imaging plane (Fig. 8c), the wave pattern was changed as a stripe-speckle mixed pattern. In sagittal images (Fig. 8d,e,f), even if changing the MEG, these three shear waves propagation patterns look almost the same, compared with coronal wave images variations. Fig. 8d was similar to an equally-spaced stripe pattern of Fig. 8a, their MEG direction were same orientation. These results thought to be because the ball-actuator has complex vibration (vibration resulting from centrifugal action), and the modes of the vibrations comprise a parallel plane to centrifugal action and a perpendicular plane to centrifugal action. Since the centrifugal force is directed along a vector between the center of rotation and the instantaneous position of the ball, the direction of motion of the actuator will be in the same direction (orthogonal to the ball's instantaneous tangential motion vector). This should make the overall motion of the actuator follow a circular path in the same plane as the motion of the ball. In sagittal images (Fig. 8d,e,f), since the imaging and the centrifugal action plane at right angle to each other, the representative displacement of sagittal imaging plane has longitudinal direction. On the other hand, in coronal images (Fig. 8a,b,c), since the imaging and the centrifugal action plane are same direction, the displacement of coronal imaging plane has longitudinal and transverse directions. Therefore, shear waves propagation pattern of coronal image could be easily changed by selecting a MEG direction. Other considerations about, although agarose-gel allows for very good depiction of shear waves, it has a low loss modulus. Thus, shear waves are not well attenuated at a distance of many wavelengths from the vibration source. To a lesser or greater degree, there is no denying that this results in wave interference patterns due to reflections off the phantom walls and bottom of the container. Fig. 9 shows a comparison between uniform phantom images and inclusion phantom images. These image planes and the MEG direction were coronal section images and the L-R MEG

direction (same as in Fig.8a). The Elastogram of the uniform phantom shows nearly homogeneous stiffness, except for the surface layer (3.0%). By comparing the magnitude image of the inclusion phantom and the elastogram of the inclusion phantom, even though the magnitude image shows nearly homogeneous image intensity, the elastogram is imaging the internal globular portion (1.25%).

4. Discussion

The new MRI-compatible ball-actuator system allowed the generation of powerful vibrations that maintained an adequate amount of displacement with high frequency vibrations. It is known that as the frequency of vibration increases, the wavelength decreases and the MRE resolution increases, while the depth of penetration of the wave decreases due to the increase in attenuation [20]. The ball-actuator system was developed to achieve coexistence of high frequency and large displacement. That said, we believe that the cause of actuator's displacement has been a confluence of various factors, including contact pressure between load (imaging object) and actuator, and so it is difficult to explain simplistically. These other "various factors" include, weight of load, viscosity of a load, volume of a load. Thus, the theoretical formula of air ball-actuator displacement can be quite complex. To reducing complexity, we debated only to the main points of the centrifugal force.

Over the years, several MRE vibration devices have been developed, each with their own characteristics. Electromechanical [1,20,21], piezoelectric [13], and remote-pneumatic [11,14,15] actuators were commonly used. In clinical application, remote-pneumatic actuators are becoming the mainstream MRE vibration device. There have been few reports on the clinical application of electromechanical and piezoelectric vibration processes. Electromechanical actuators exploit the interaction between the static magnetic field B_0 and an annular coil supplied with alternating currents. Electromagnetically-induced periodic tilt force is transformed for mechanical actuation using a pivoted rod. The mechanical structure of an electromechanical actuator precludes installing an actuator in an arbitrary place of a human body. On the other hand, remote-pneumatic actuators, a widely used method of creating the required vibrations for MRE. Commonly-used a big stethoscope-like driver can be easily manipulated, and the portion of the driver system actually in the vicinity of the patient is made out of non-magnetic materials that do not produce MR image artifacts [4]. Installation of a driver for the human body is easier for a remote-pneumatic actuator than an electromechanical actuator. As far as the low acoustic frequency range goes, output displacement of a remote-pneumatic actuator is larger than a piezoelectric actuator. For the reasons listed above, remote-pneumatic actuators are viable in clinical application. Having said that, remote-pneumatic actuators have a few drawbacks. The vibration source of a remote-pneumatic actuator, an acoustic speaker, has to be separated from the MRI magnet, so it needs a long connecting tube. A loss of energy-transfer arises because a remote-pneumatic actuator requires a safe distance between an

acoustic speaker and a big stethoscope-like driver using a long connecting tube. If properly designed the pneumatic pressure source (acoustic speaker) can be located within a few meters of the MR magnet, it reduce the loss of energy-transfer. In another drawback, if the vibration frequency increases (150Hz or more), the output of a remote-pneumatic actuator makes it difficult to obtain an adequate amount of wave penetration displacements for in vivo application. A remote-pneumatic actuator is restricted in a method for low vibration frequency MRE.

The results obtained from the ball-actuator performance assessment experiments indicate that even though the vibration frequency increases, the ball-actuator can maintain an adequate amount of displacement. In addition, because moving parts of ball-actuator is always cooled by an inflow compressed air, the ball-actuator does not generate heat. However, the ball-actuator does need a powerful compressor to achieve high frequency vibration (250Hz or more). The discharge rate of compressor for this experiment was 72l/min and a compressor had one storage tank (30l). Under these components, this compressor (0.75kW, 72l/min) was unable to accept the discharge rate of over 100l/min. Therefore, high frequency vibration (250Hz or more) was difficult by using a low-power compressor. In order to attain high frequency vibration, high-power compressor (2.0kW or more) with the discharge rate of 200 or more l/min is required. Although having said that, in this experiment, by contrast, was aimed at testing technology that will allow the ball-actuator to make an elastogram.

From the results of phantom MRE experiments, the ball-actuator produces shear waves, which can be used to generate 200Hz vibration frequency MRE. The ball-actuator design avoids the use of any materials that could disturb the homogeneous field of the MRI magnet. Furthermore, the ball-actuator can be installed to the imaging object in a direct way and generates powerful vibrations at that area. Because the vibration source of a ball-actuator and the vibration transmission parts are the same, loss of energy-transfer is very limited in the ball-actuator. In an agarose gel phantom with stiff spherical inserts, the inserts could be identified in the calculated shear stiffness map. The silencer mitigates ball-actuator exhaust noise, but exhaust efficiency and revolution speed falls. To achieve high vibration frequency, it is realistic to avoid silencer and put earplugs instead. The exhaust noise is attenuated by earplugs or non-magnetic ear muffs, as overall MRE loud noises (include MRI scan noise) in MRI scan room.

Typically, in classical MRE experiments do not use continuous mechanical vibration of the subject, and only a finite duration of vibration is send prior to each signal acquisition. However, since air ball-actuator requires the inertial ramp time (whenever it restarts, the inertial ramp time is required for air ball-actuator), the vibration which air ball-actuator makes becomes continuously. Recently, some clinical studies exploit simultaneous multi-frequency vibration for mapping in vivo viscoelastic properties of organs such as liver [22], in order to provide a more efficient data acquisition for different frequencies. The ball-actuator which generates continuous mechanical

vibration (it generates only one frequency component) does not allow for such multi-frequency vibration MR elastography.

Most recently, there was a report of the prostate MRE by piezoceramic actuator excitation [23] or remote-hydraulic actuator excitation [24]. This piezoceramic actuator was using coupled mechanically to an endorectal RF receiver coil. When the unit of piezoceramic actuator is replaced to ball-actuator, the size of entire vibration unit may become compact. The remote-hydraulic actuator, on the other hand, it was using an electromagnetic actuator with a remote-hydraulic transmission system. Since the ball-actuator can be vibrating directly to the object, if the vibration mechanical part was replaced to ball-actuator; the energy loss of vibration transmission may be less than remote-hydraulic actuator. However, in either case, the ball-actuator makes continuous vibration throughout the entire MRE acquisition (one vibration phase offset). For clinical application of air ball-actuator, in some parts of the human body, the user might want to give it some thought for the continuous vibration.

5. Conclusion

We demonstrated MR Elastography in agarose gel phantom experiments by using a new MRI-compatible MRE actuator. The MRI-compatible air ball-actuator is a new technique that directly transmits centrifugal vibrations through a ball-actuator body. From the results of phantom MRE experiments, the ball-actuator produces reasonable shear waves. In essence, the MRI-compatible air ball-actuator system can be used to achieve a high vibration frequency.

Acknowledgment

This work was supported in part by a Grant-in-Aid for Scientific Research (22791211).

References

1. Muthupillai R, Lomas DJ, Rossman PJ, Greenleaf JF, Manduca A, Ehman RL. Magnetic resonance elastography by direct visualization of propagating acoustic strain waves. Science 1995;269(5232):1854-1857.
2. Muthupillai R, Rossman PJ, Lomas DJ, Greenleaf JF, Riederer SJ, Ehman RL. Magnetic resonance imaging of transverse acoustic strain waves. Magn Reson Med 1996;36(2):266-274.
3. Muthupillai R, Ehman RL. Magnetic resonance elastography. Nature medicine 1996;2(5):601-603.
4. Mariappan YK, Glaser KJ, Ehman RL. Magnetic resonance elastography: a review. Clinical anatomy (New York, NY 2010;23(5):497-511.
5. Sinkus R, Lorenzen J, Schrader D, Lorenzen M, Dargatz M, Holz D. High-resolution tensor MR elastography for breast tumour detection. Physics in medicine and biology

2000;45(6):1649-1664.

6. Plewes DB, Bishop J, Samani A, Sciarretta J. Visualization and quantification of breast cancer biomechanical properties with magnetic resonance elastography. Physics in medicine and biology 2000;45(6):1591-1610.
7. Lopez O, Amrami KK, Manduca A, Rossman PJ, Ehman RL. Developments in dynamic MR elastography for in vitro biomechanical assessment of hyaline cartilage under high-frequency cyclical shear. J Magn Reson Imaging 2007;25(2):310-320.
8. Manduca A, Oliphant TE, Dresner MA, Mahowald JL, Kruse SA, Amromin E, Felmlee JP, Greenleaf JF, Ehman RL. Magnetic resonance elastography: non-invasive mapping of tissue elasticity. Medical image analysis 2001;5(4):237-254.
9. McKnight AL, Kugel JL, Rossman PJ, Manduca A, Hartmann LC, Ehman RL. MR elastography of breast cancer: preliminary results. Ajr 2002;178(6):1411-1417.
10. Lorenzen J, Sinkus R, Lorenzen M, Dargatz M, Leussler C, Roschmann P, Adam G. MR elastography of the breast:preliminary clinical results. Rofo 2002;174(7):830-834.
11. Rouviere O, Yin M, Dresner MA, Rossman PJ, Burgart LJ, Fidler JL, Ehman RL. MR elastography of the liver: preliminary results. Radiology 2006;240(2):440-448.
12. Kemper J, Sinkus R, Lorenzen J, Nolte-Ernsting C, Stork A, Adam G. MR elastography of the prostate: initial in-vivo application. Rofo 2004;176(8):1094-1099.
13. Othman SF, Xu H, Royston TJ, Magin RL. Microscopic magnetic resonance elastography (microMRE). Magn Reson Med 2005;54(3):605-615.
14. Latta P, Gruwel ML, Debergue P, Matwiy B, Sboto-Frankenstein UN, Tomanek B. Convertible pneumatic actuator for magnetic resonance elastography of the brain. Magnetic resonance imaging 2011;29(1):147-152.
15. Bensamoun SF, Ringleb SI, Littrell L, Chen Q, Brennan M, Ehman RL, An KN. Determination of thigh muscle stiffness using magnetic resonance elastography. J Magn Reson Imaging 2006;23(2):242-247.
16. Venkatesh SK, Yin M, Glockner JF, Takahashi N, Araoz PA, Talwalkar JA, Ehman RL. MR elastography of liver tumors: preliminary results. Ajr 2008;190(6):1534-1540.
17. Huwart L, Salameh N, ter Beek L, Vicaut E, Peeters F, Sinkus R, Van Beers BE. MR elastography of liver fibrosis: preliminary results comparing spin-echo and echo-planar imaging. European radiology 2008;18(11):2535-2541.
18. Papazoglou S, Rump J, Braun J, Sack I. Shear wave group velocity inversion in MR elastography of human skeletal muscle. Magn Reson Med 2006;56(3):489-497.
19. Uffmann K, Maderwald S, Ajaj W, Galban CG, Mateiescu S, Quick HH, Ladd ME. In vivo elasticity measurements of extremity skeletal muscle with MR elastography. NMR in biomedicine 2004;17(4):181-190.

20. Mariappan YK, Rossman PJ, Glaser KJ, Manduca A, Ehman RL. Magnetic resonance elastography with a phased-array acoustic driver system. Magn Reson Med 2009;61(3):678-685.
21. Braun J, Braun K, Sack I. Electromagnetic actuator for generating variably oriented shear waves in MR elastography. Magn Reson Med 2003;50(1):220-222.
22. Asbach P, Klatt D, Hamhaber U, Braun J, Somasundaram R, Hamm B, Sack I. Assessment of liver viscoelasticity using multifrequency MR elastography. Magn Reson Med 2008;60(2):373-379.
23. Arani A, Plewes D, Krieger A, Chopra R. The feasibility of endorectal MR elastography for prostate cancer localization. Magn Reson Med. 2011;66(6):1649-1657.
24. Sahebjavaher RS, Baghani A, Honarvar M, Sinkus R, Salcudean SE. Transperineal prostate MR elastography: Initial in vivo results. Magn Reson Med. 2012 [Epub ahead of print]

Figure legends

FIG. 1. Photographs of the ball-actuators. a: A picture of the main unit of the ball-actuator. [1]tube connector, [2]internal ball, [3]raceway ring, [4]optical-fiber sensor, [5]silencer. b: Fixation to a plastic phantom container. c: A schematic of the basic concepts of the ball-actuator.

FIG. 2. Calculated vibration force from each ball-weight and ball-diameter by ball type. Each ball revolution is 6000 rpm (vibration frequency is 100Hz). 7/16: 7/16 inch diameter, 5/16: 5/16 inch diameter, AC: alumina ceramic, PTFE: polytetrafluoroethylene, POM: polyoxymethylene, PEEK: polyetheretherketone.

FIG. 3. Ball-actuator MRE system. Compressed air generated by a compressor is dehydrated by a mist separator. The dehydrated air is controlled for flow volume by a high-precision regulator, and introduced into the ball-actuator. A four-channel optical signal is generated by optical-fiber sensors. Optical signals are converted by a signal converter to a transistor-transistor logic (TTL) signal. Four-channel TTL signals are selected by the channel selector to a one-channel TTL signal. The selected one-channel TTL signal is used to trigger an MRI signal. Selection of a TTL signal by using the channel selector is synonymous with selection of the vibration phase offset.

FIG. 4. a: Self-modified spin echo MRE sequence. The MEG was applied symmetrically around a refocusing pulse and can being applied in any gradient direction. The period of external vibration and the period of MEG were in agreement. b: The ball-actuator system was generating the synchronization pulse for the MRI scanner. When the acquisition of MRI is ready and waiting, the trigger signal of ball-actuator becomes effective.

FIG. 5. a: The triaxial accelerations of the ball-actuator were measured by a tri-axis XYZ accelerometer. Arrowed lines indicate the accelerometer coordinate system, and it was loaded condition (impact absorption rubber mat). b: The displacements measured with the ball-actuator were in a loaded condition (approximately agarose-gel 2.8kg). It's made from a 1.0% agarose gel (weight %) was poured into a rigid acrylic container.

FIG. 6. Ball-actuator performance assessment experiments. a: Comparison of frequency (rpm / sixty-seconds) of each internal ball. In all types of internal balls, the frequency increased with increased air flow volume. b: Comparison of triaxial accelerations. The internal ball was 5/16 PEEK. Because the internal ball was rotate in accelerometer's Y-Z plane, the X-axis had a smaller amount of acceleration, compared with Y- or Z-axis. c: Comparison of displacement for each internal ball. Excluding the sympathetic vibration of the ball actuator (approx. 35Hz, 70Hz), the ball-actuator was able to maintain a certain value of displacement.

FIG. 7. Shear wave images in homogenous agarose gel phantoms with different vibration frequencies and different vibration phase offsets. At both vibration frequencies, when the vibration offset 0 (or $\pi/2$) of the wave image is compared with the vibration offset π (or $3\pi/2$), the pattern of the shear wave propagation in the agarose phantom is inverted. Arrowed line indicates the direction of MEG.

FIG. 8. Comparison of the homogenous agarose gel phantom wave image of the imaging plane and the direction of MEG. Vibration frequency was 160Hz. a,b,c: Coronal section images. d,e,f: Sagittal section images. Arrowed line indicates the direction of MEG.

FIG. 9. Comparison of uniform phantom images and inclusion phantom images. A uniform phantom made from a 1.0% agarose gel (weight %) was poured into a semi-rigid plastic container. An inclusion phantom spherical stiff inclusion (1.25% agarose gel) of 30mm diameter was enclosed in the center. A stiff incursion could be identified in the inclusion phantom elastogram.

Table

Abbreviation	Material	Ball diameter [inch]	Rolling radius [mm]	Specific weight	Weight [g]
5/16 PEEK	Polyether ether ketone	5/16	14.3	1.32	0.35
5/16 POM	Polyxymethylene	5/16	14.3	1.42	0.37
5/16 PTFE	Polytetrafluoroethylene	5/16	14.3	2.20	0.58
5/16 AC	Alumina ceramic	5/16	14.3	3.60	0.94
7/16 POM	Polyxymethylene	7/16	12.5	1.42	1.02
7/16 PTFE	Polytetrafluoroethylene	7/16	12.5	2.20	1.58
7/16 AC	Alumina ceramic	7/16	12.5	3.60	2.59

Table 1

Weight of the internal ball using the ball-vibrator and the corresponding diameter sizes. If the diameter of the internal ball is increased, the rolling radius of the internal ball decreases.

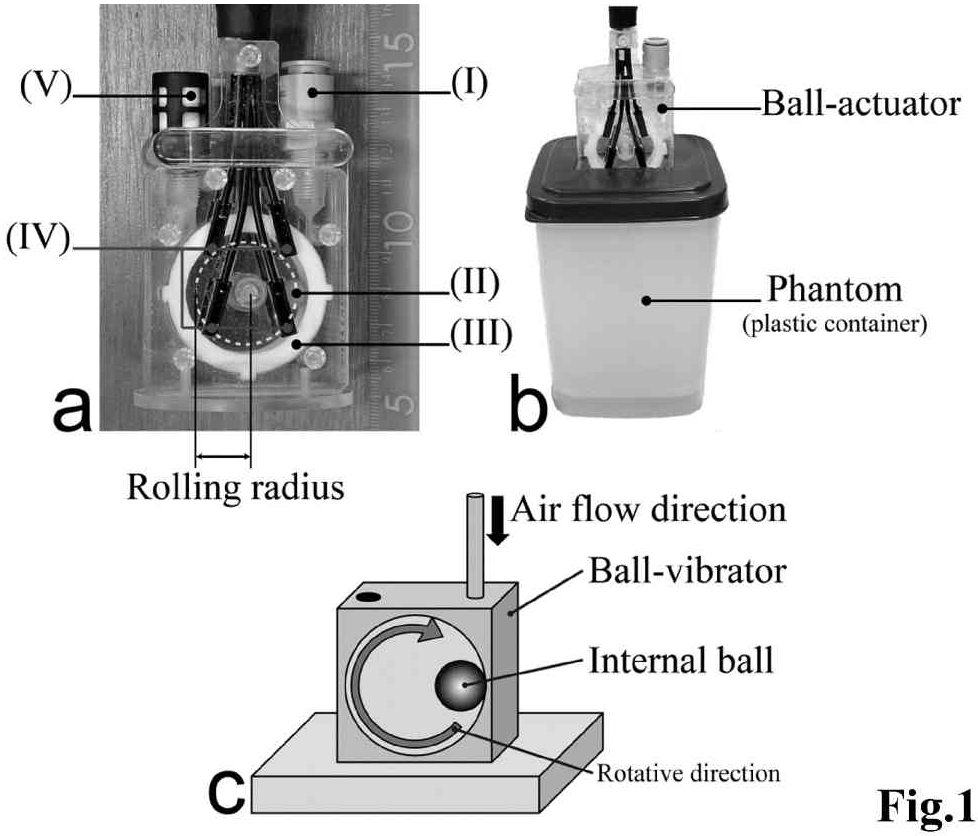
(V)
(I)
(IV)
(II)
(III)
a
Rolling radius
Ball-actuator
Phantom
(plastic container)
b
Air flow direction
Ball-vibrator
Internal ball
Rotative direction
c

Fig.1

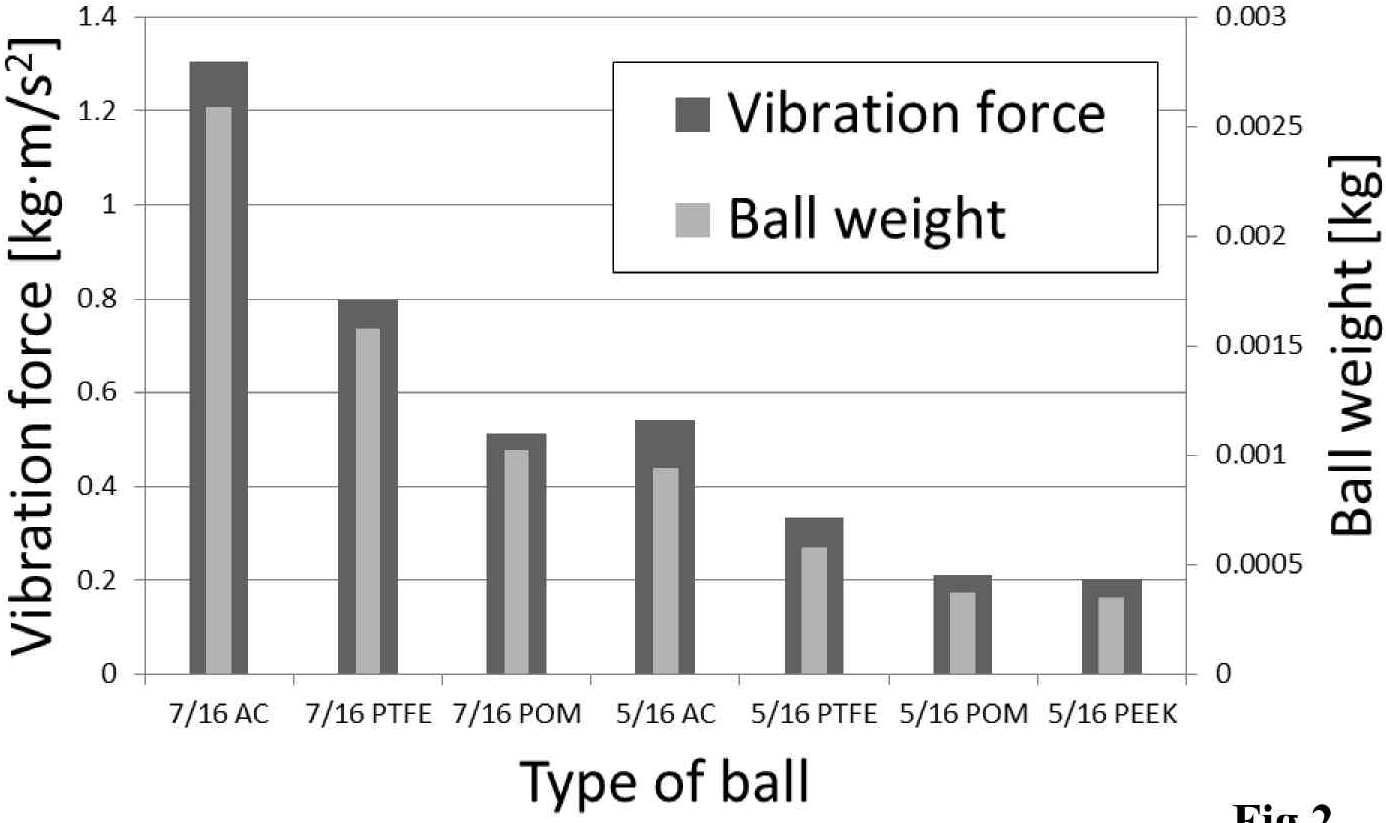
Vibration force [kg·m/s²]
Ball weight [kg]
Vibration force
Ball weight
1.4
1.2
1
0.8
0.6
0.4
0.2
0
0.003
0.0025
0.002
0.0015
0.001
0.0005
0
7/16 AC
7/16 PTFE
7/16 POM
5/16 AC
5/16 PTFE
5/16 POM
5/16 PEEK
Type of ball

Fig.2

(I) Compressor

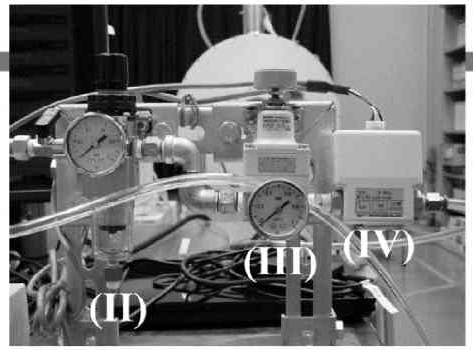

(II) Mist separator
(III) High-precision regulator
(IV) Thermal mass flowmeter

compressed air →

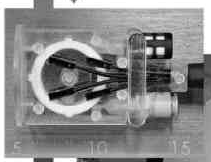

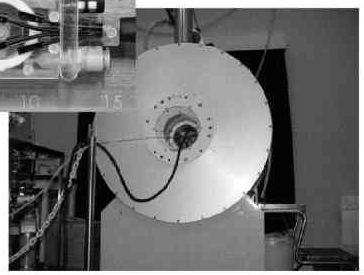

Ball-vibrator, MRI magnet

MRI system

selected 1ch TTL signal ←

4ch optical signal →

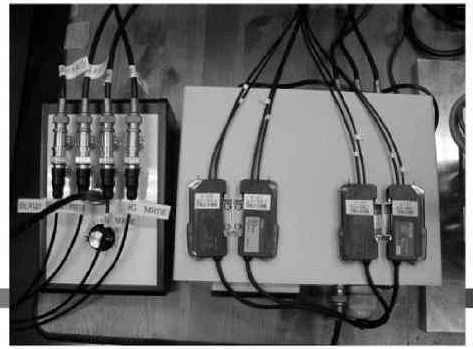

(V) Optical signal operating system
- optical signal - TTL converter
- channel selector

Fig.3

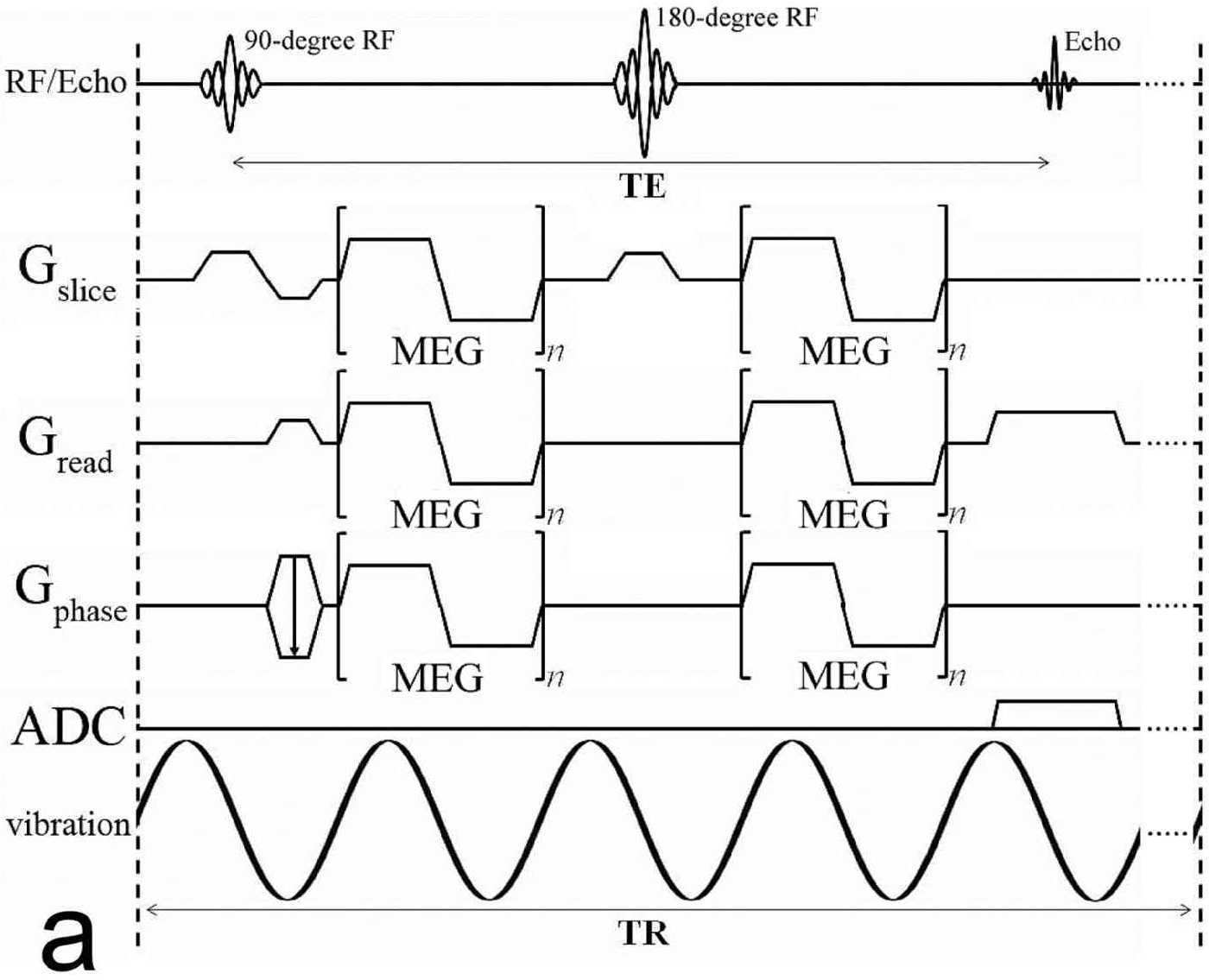
RF/Echo
90-degree RF
180-degree RF
Echo
TE
G slice
MEG
n
G read
G phase
ADC
vibration
TR
a

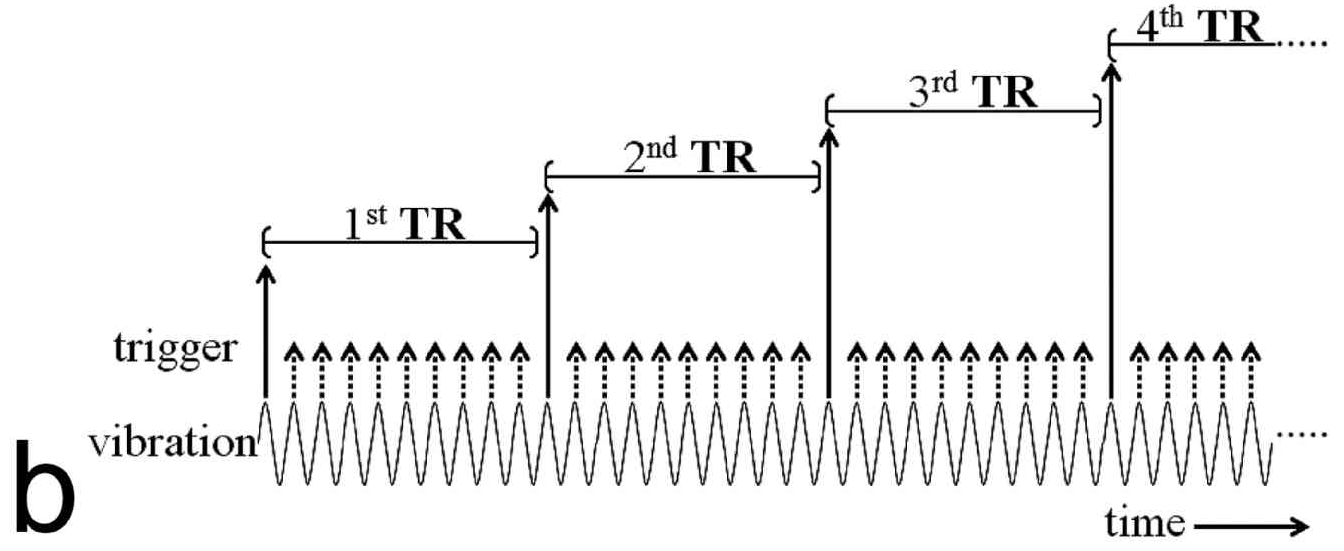
1st TR
2nd TR
3rd TR
4th TR
trigger
vibration
time
b

Fig.4

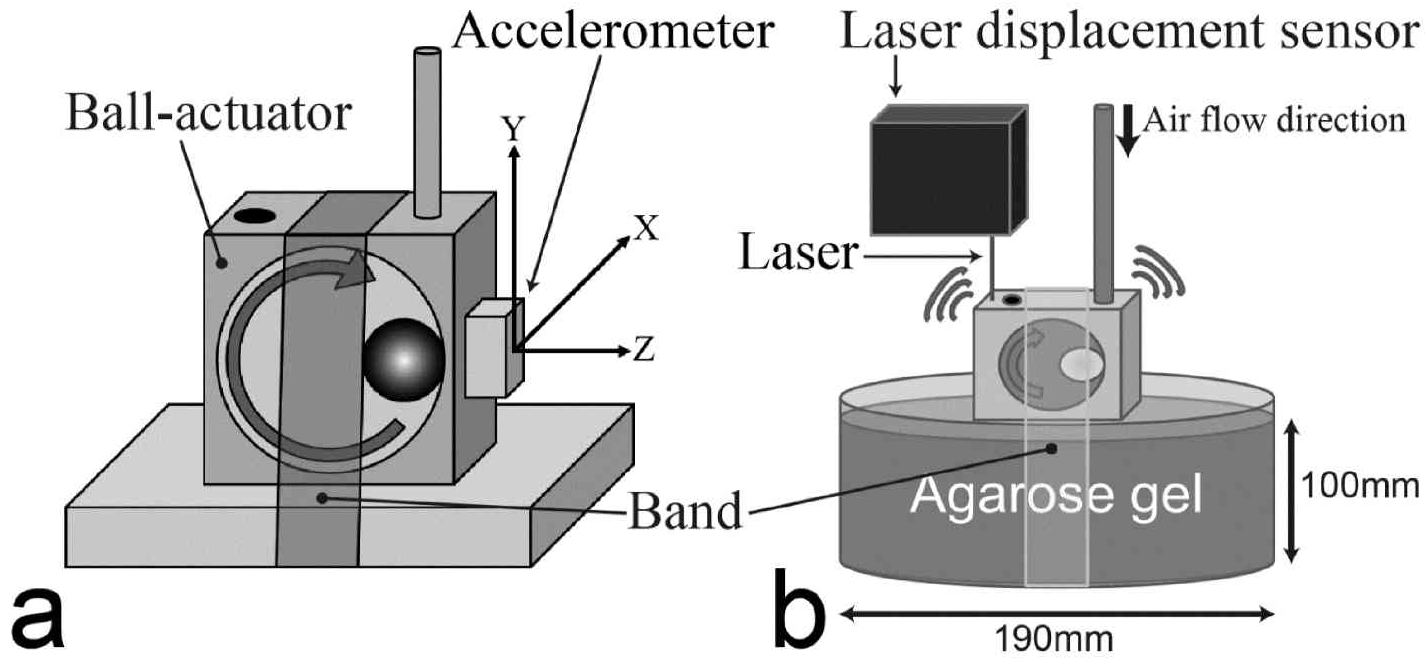
Accelerometer
Laser displacement sensor
Ball-actuator
Y
X
Z
Air flow direction
Laser
Band
Agarose gel
100mm
a
b
190mm

Fig.5

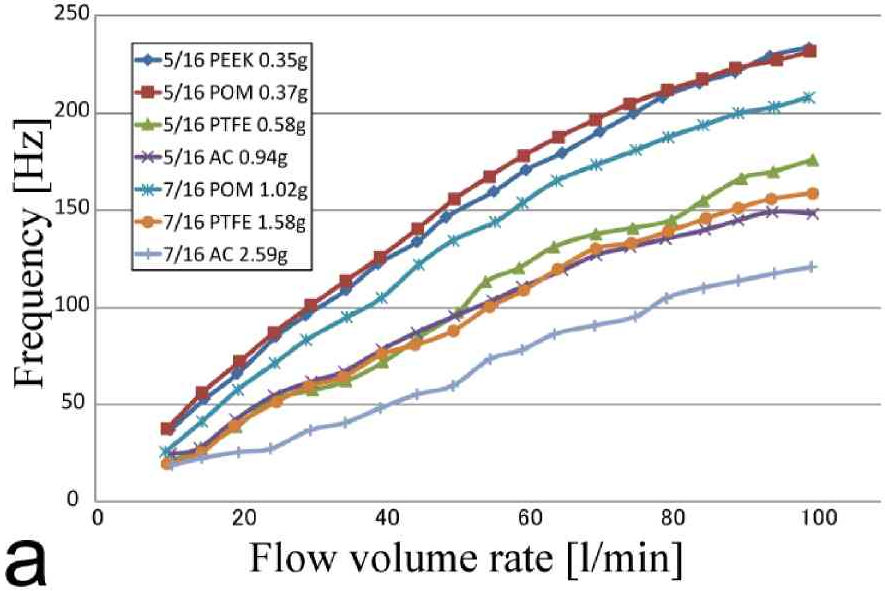
5/16 PEEK 0.35g
5/16 POM 0.37g
5/16 PTFE 0.58g
5/16 AC 0.94g
7/16 POM 1.02g
7/16 PTFE 1.58g
7/16 AC 2.59g
Frequency [Hz]
Flow volume rate [l/min]
0
50
100
150
200
250
0
20
40
60
80
100

a

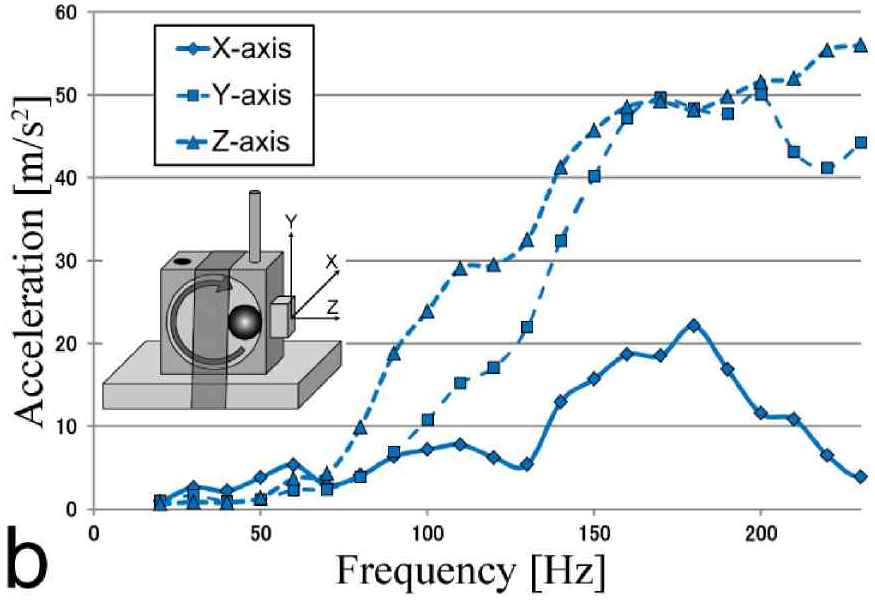
X-axis
Y-axis
Z-axis
Acceleration [m/s²]
Frequency [Hz]
Y
X
Z
0
10
20
30
40
50
60
0
50
100
150
200

b

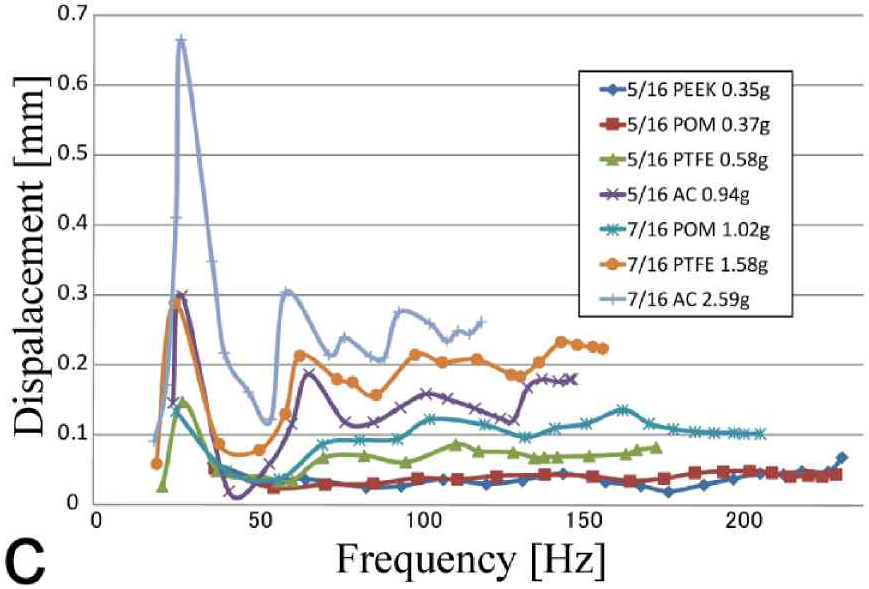
5/16 PEEK 0.35g
5/16 POM 0.37g
5/16 PTFE 0.58g
5/16 AC 0.94g
7/16 POM 1.02g
7/16 PTFE 1.58g
7/16 AC 2.59g
Dispalacement [mm]
Frequency [Hz]
0
0.1
0.2
0.3
0.4
0.5
0.6
0.7
0
50
100
150
200

c

Fig.6

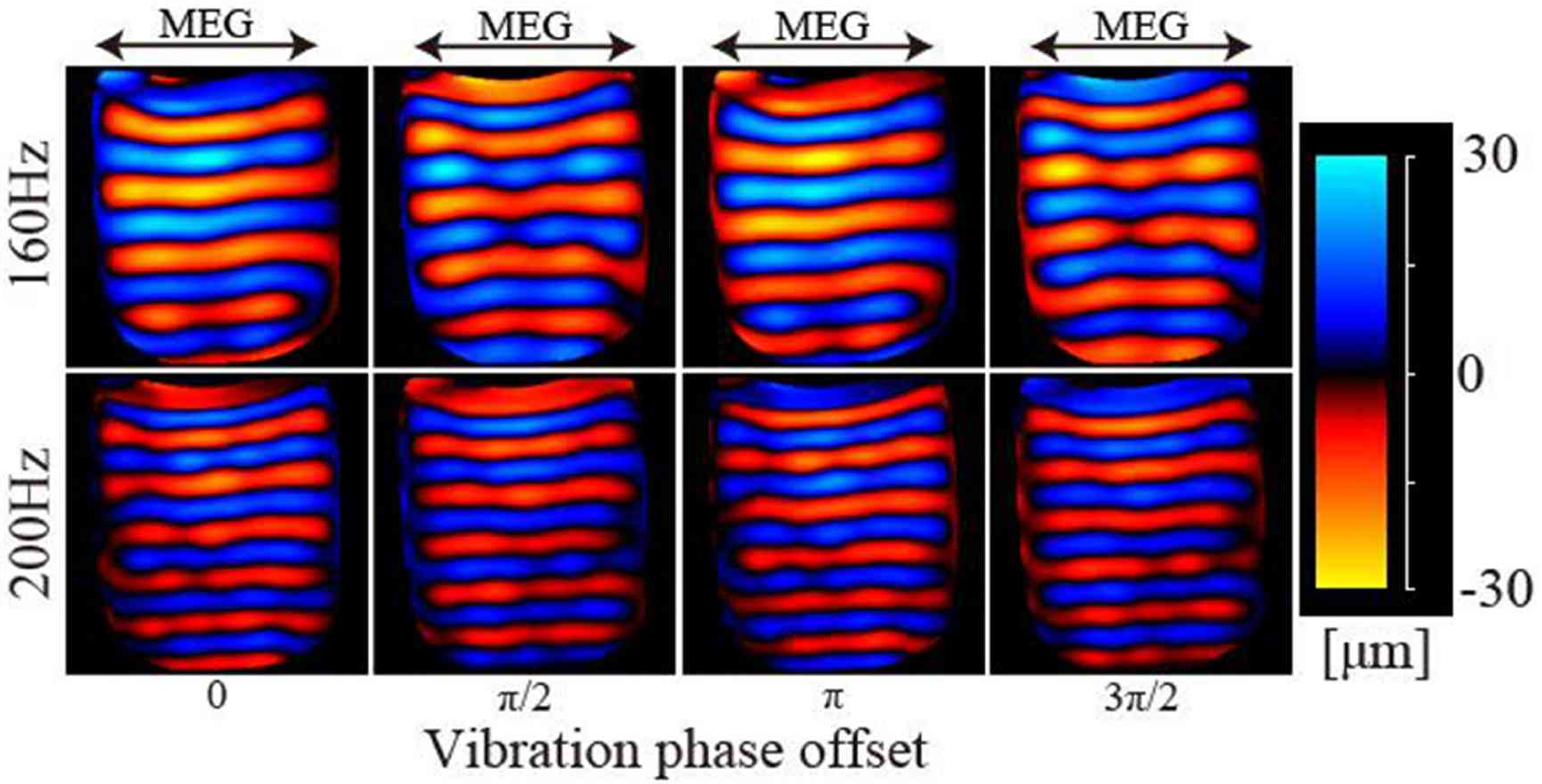
MEG
MEG
MEG
MEG
160Hz
200Hz
30
0
-30
[μm]
0
π/2
π
3π/2
Vibration phase offset

Fig.7

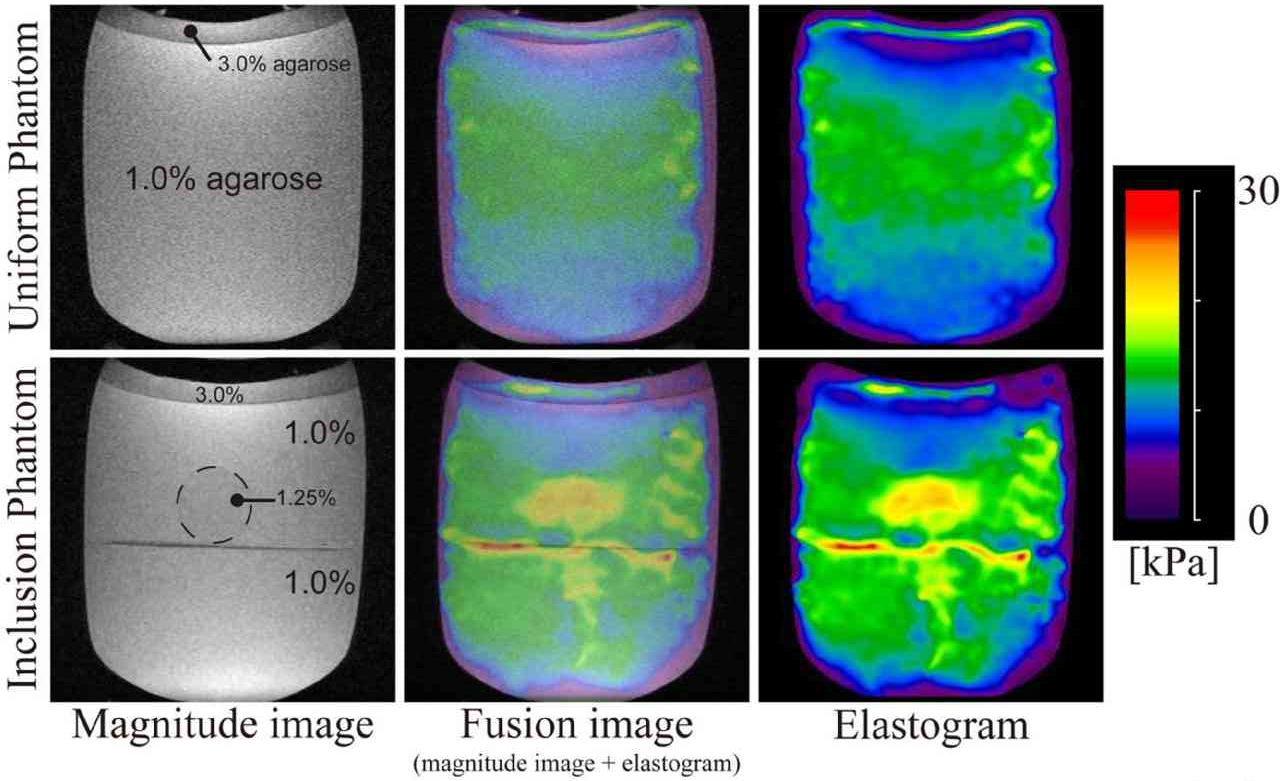
Uniform Phantom
Inclusion Phantom
3.0% agarose
1.0% agarose
3.0%
1.0%
1.25%
1.0%
30
0
[kPa]
Magnitude image
Fusion image
(magnitude image + elastogram)
Elastogram

Fig.9